Appl. Phys. B 55, 279–290 (1992)

Applied Physics B Photophysics and Laser Chemistry

Atomic Spectroscopy with Squeezed Light for Sensitivity Beyond the Vacuum-State Limit

E. S. Polzik, J. Carri, and H. J. Kimble

Norman Bridge Laboratory of Physics 12–33, California Institute of Technology, Pasadena, CA 91125, USA
(Fax: +1-818/793-9506)

Received 16 March 1992/Accepted 4 May 1992

Abstract. A frequency tunable source of squeezed light has been developed which is suitable for a variety of spectroscopic applications. In initial experiments continuous tunability over a range of 2 GHz has been achieved with a directly observed nonclassical noise reduction of 6 dB relative to the vacuum-state limit in a balanced homodyne detector. A process of light-induced absorption in the nonlinear crystal has been identified as the principal loss mechanism which prevents the observation of yet larger degrees of squeezing. Although our source is potentially broadly tunable over the range of wavelengths from 840 to 970 nm, the current research centers on the performance at 852 nm for spectroscopy of the D_2 line of atomic cesium. For frequency-modulated (FM) saturation spectroscopy in a vapor cell, an improvement of 3.1 dB in sensitivity relative to the usual quantum limit is demonstrated for the detection of Doppler-free resonances. When corrected for the thermal noise of the detector, the enhancement in signal-to-noise ratio brought by the squeezed field is 3.8 dB relative to the shot-noise limit set by the vacuum fluctuations of the probe field.

PACS: 42.62.Fi, 32.80.–t, 42.50.Dv

Contemporary with the first experiments to generate squeezed light have been theoretical investigations of a variety of problems related to the interaction of squeezed light with atoms. For example, Milburn [1] showed that the collapse time for the inversion of an atom driven by squeezed light is different from that of an atom driven by a coherent field. In a landmark paper, Gardiner [2] found that the spontaneous emission from an atom embedded in a squeezed vacuum is characterized by two transverse decay rates which reflect the enhanced and diminished fluctuations of a squeezed state relative to the vacuum field. The resulting sub- and super-natural linewidths have subsequently made ubiquitous appearances of diverse problems in optical physics, including the spectra of resonance fluorescence [3, 4] and the photon echoes from a sequence of coherent and squeezed pulses [5]. The modification of atomic level shifts by a squeezed vacuum has also been considered [6]. Beyond the problem of an atom in "free-space" illuminated by 4π sterradians of squeezed light, a variety of new effects have been predicted for atoms coupled to a resonant cavity driven by squeezed light. The nonclassical fluctuations of a squeezed field can have profound effects on the phenomenology of cavity QED both in the regime of strong [1, 7] and of weak coupling [8], as well as on the behavior of lasers [9] and of bistable systems [10].

In addition to fundamental alterations of atomic radiative processes, another potentially exciting avenue for the application of squeezed light in atomic physics is that of precision measurement. Squeezed light has already been successfully employed to achieve sensitivity beyond the vacuum-state (or shot-noise) limit in Mach-Zehnder [11] and polarization interferometers [12] and for the detection of directly encoded amplitude modulation [13]. The utilization of squeezed light for atomic and molecular spectroscopic measurements also holds promise for enhancements in sensitivity beyond the usual quantum limit [14].

Motivated by these and other exciting perspectives, we have constructed a broadly tunable source of squeezed light for spectroscopic applications in atomic physics [38]. In this paper we describe our cw source of squeezed-light which is based on an optical parametric oscillator operated below threshold. For wavelengths around 855 nm, we report observations of quantum noise reduction of 6 dB below the vacuum-state limit for the photocurrent fluctuations in a balanced homodyne detector. The implementation of this source for FM saturation spectroscopy is described with an improvement in sensitivity of 3.1 dB beyond the usual quantum limit [15–17] achieved for the detection of Doppler-free resonances in atomic cesium. After correction is made for the thermal noise of the photodetection electronics, the enhancement of sensitivity in FM spectroscopy becomes 3.8 dB.

1 Frequency Tunable Source of Squeezed Light

A *General Considerations*

For our work a subthreshold optical parametric oscillator (OPO) has been developed as a frequency tunable source of squeezed light [18]. The spontaneous parametric fluorescence produced by degenerate down conversion into a subharmonic mode of the OPO leads to a squeezed field of zero mean amplitude emitted into the external reservoir. For an ideal single-sided cavity without internal losses, the spectrum of squeezing for the output field is defined to be [19–21]

$$S(\Omega,\theta) = 2\Gamma \int_{-\infty}^{\infty} d\tau \langle : \hat{X}_\theta(t), \hat{X}_\theta(t+\tau) : \rangle e^{-i\Omega\tau}, \quad (1)$$

where Γ is the cavity linewidth (HWHM) and the quadrature phase amplitude $\hat{X}_\theta(t)$ of the intracavity field $\hat{a}$ is defined by

$$\hat{X}_\theta(t) = e^{-i\theta}\hat{a}(t) + e^{i\theta}\hat{a}^\dagger(t). \quad (2)$$

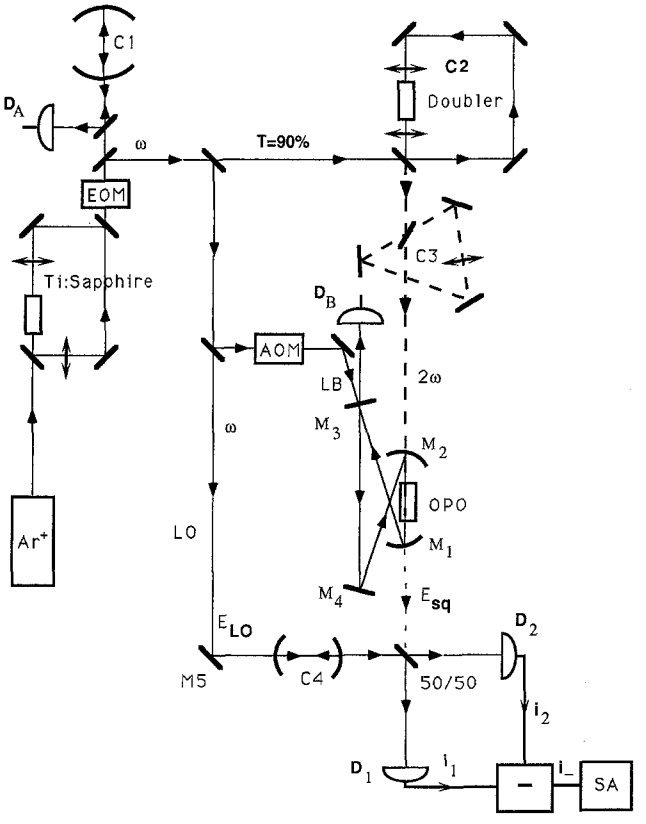

Fig. 1. Frequency tunable source of squeezed light for wavelengths around 855 nm. The principal components of the system are as follows: C1 – reference cavity for frequency stabilization of the titanium-sapphire laser and hence for all other fields and cavities of the system; C2 – external frequency doubling cavity; C3 – transfer cavity serving as a reference for the spatial mode of the blue pump beam; C4 – mode-cleaning cavity for the local oscillator beam (LO). The resonance of the optical parametric oscillator (OPO) is actively locked with a locking beam (LB). Quantum noise of the squeezed beam E_{sq} is detected with the balanced homodyne detector formed by D_1, D_2

The colons in (1) denote normal and time ordering; S is then such that $S(\Omega,\theta_-) \equiv S_- \rightarrowtail -1$ for the optimally squeezed quadrature, while necessarily $S(\Omega,\theta_+) \equiv S_+ \rightarrowtail \infty$ for an ideal squeezed state in the limit of large squeezing. For a subthreshold OPO the spectrum of squeezing is given by [19–21]

$$S_\pm(\Omega) = \pm\frac{4(P_2/P_{20})^{1/2}}{(\Omega/\Gamma)^2 + [1 \mp (P_2/P_{20})^{1/2}]^2}, \quad (3)$$

where P_2 is the pump power of the field at 2ω with P_{20} as the threshold pump power for the OPO ($P_2/P_{20} < 1$).

To measure the degree of squeezing of the output field from the OPO, we employ a balanced homodyne detector [21, 22] for which the squeezed-vacuum input is combined with an intense local oscillator beam at a 50/50 beamsplitter. As shown in Fig. 1, the two outputs from the beamsplitter are directed to photodetectors (D_1, D_2) to generate photocurrents (i_1, i_2) which are then subtracted to yield the difference photocurrent i_-. The spectral density $\Phi(\Omega,\theta)$ for the fluctuations of i_- is measured with a spectrum analyzer and is related to the spectrum of squeezing $S(\Omega,\theta)$ by [18, 21]

$$\Phi(\Omega,\theta) = \Phi_0[1 + \xi\varrho S(\Omega,\theta)], \quad (4)$$

where Φ_0 is the spectral density for a vacuum-state input ($S = 0$). The efficiency with which the squeezed field escapes from the OPO cavity is given by $\varrho = T/(T+L)$, with T as the transmission of the OPO output coupler mirror M_1 and L as all other intracavity losses. The efficiency factor $\xi = \zeta\alpha\eta^2$ includes ζ as the propagation efficiency from the OPO output to the balanced detector, α as the detector quantum efficiency, and η as the homodyne efficiency describing the spatial overlap of the mode of the local oscillator field with that of the squeezed-vacuum field. Measurement of the ratio $\Phi(\Omega,\theta)/\Phi_0$ together with the individual efficiency factors allows us to infer $S(\Omega,\theta)$ for the OPO.

B *Experimental Configuration*

A schematic diagram of our source of tunable squeezed light is shown in Fig. 1. A single-frequency titanium-sapphire laser serves as the primary source, with the frequency of the laser locked to a stable reference cavity C1 via a standard FM-sideband technique [23]. For this purpose an electrooptic modulator (EOM) encodes FM sidebands on the laser output at a frequency of 27 MHz. The rms linewidth of the locked laser is measured to be about 30 kHz. 90% of the laser output at frequency ω is directed to a frequency-doubling cavity C2 to generate a blue pumping beam at 2ω for the OPO. The doubling cavity contains a potassium niobate ($KNbO_3$) crystal as the nonlinear element and is frequency locked to the incident laser with the help of the same 27 MHz sidebands. For an input pump of 1.35 W at ω, this system is capable of producing 650 mW of cw tunable light around 427 nm [24].

In the design of the OPO cavity, we have attempted to achieve both frequency tunability and a large degree of squeezing. Since a scheme for which both the pump field and the down converted field are simultaneously resonant in the OPO is tightly constrained by the requirements of satisfying boundary conditions on the mirrors as well as the

generally incommensurate phase-matching conditions inside the crystal [18, 25], we have chosen to have only the down-converted field resonant and to use the pump in a single-pass configuration. Having made this choice, we are then obliged to use a ring cavity to maximize squeezing given the fact that crystal losses are the dominate losses in our cavity. This is clear since the degree of squeezing of the external field is limited to a value $S_{\text{ext}} = \varrho S$ (with S as the squeezing spectrum for an ideal single-sided cavity [19–21] and S_{ext} as the spectrum for a cavity with nonzero internal losses). For a cavity with the nonlinear crystal as the major source of dissipation, the round trip losses for a ring cavity are two times smaller than for a standing-wave cavity and hence $(1-\varrho)$ is approximately 2 times smaller for the ring for a given value of T.

The actual OPO cavity is a four-mirror folded cavity with two curved (M1, M2) and two plain (M3, M4) mirrors (Fig. 1). To minimize astigmatism, we chose a geometry with the smallest folding angle (3 degrees) allowed by the dimensions of the crystal and the mirror radii. Calculated astigmatism in this case is negligible provided the cavity is operated around the middle of the stability range. The nonlinear medium at the waist between mirrors (M1,M2) is an a-cut potassium niobate crystal of 10 mm length. For down conversion to wavelengths around 855 nm, potassium niobate can be temperature tuned and noncritically phase-matched with a temperature width for fixed frequency of about 0.3K (FWHM) for our 10 mm crystal. The crystal was mounted on a Peltier cooler as the active element in a temperature controller to provide temperature stability of a few mK.

A considerable effort has been invested to minimize IR losses in the OPO cavity. Low-loss AR coatings for the crystal surfaces [26] and the mirrors [27] together with the high quality of the crystal itself [28] resulted in total round-trip passive cavity loss of $L = 3 \times 10^{-3}$ (excluding the output coupler transmission and the nonlinear light-induced losses described in Sect. C below). The choices for the radii of curvature of the fold mirrors and for the total cavity length are determined as a trade-off between the requirements on the one hand for optimum beam waist in the crystal and for the smallest possible cavity length l (for large squeezing bandwidth suitable for spectroscopy) and on the other hand the need to keep the folding angle θ as small as possible to minimize various beam aberrations. Our choices are that (M1, M2) are of radii $R = 50\,\text{mm}$. The total cavity length $l = 0.5\,\text{m}$ and the waist in the crystal $w_0 = 20\,\mu\text{m}$. The single-pass nonlinear conversion coefficient $E_{NL} \equiv P_{430}/P_{860}^2$ is measured directly for our cavity geometry by replacing the output coupler M1 with a transparent (AR coated) substrate of the same curvature and dimensions; we find $E_{NL} = 0.016\,\text{W}^{-1}$. This value of E_{NL} together with the transmission $T = 0.105$ for the output coupler M1 and the total loss $L = 3 \times 10^{-3}$ allows us to calculate the expected threshold pump power P_{20} for the OPO as [18, 29]

$$P_{20} = \frac{(T+L)^2}{4E_{\text{NL}}} \cong 0.18\,\text{W}. \tag{5}$$

For efficient pumping of the OPO, the blue beam generated in the doubling cavity C2 has to be precisely modematched to the spatial mode of the OPO cavity. Unfortunately there is no straightforward means to accomplish this in a singly resonant OPO because the mirrors (M1–M4) are largely transparent to the blue pump and do not define a spatially overlapping cavity mode for the pump beam. To achieve good modematching, we use the following trick. A beam at the infrared wavelength (not shown in Fig. 1) is injected through the mirror M1 (the output coupler of the OPO) in a direction counterpropagating to the sense of circulation drawn in Fig. 1. This injected IR beam is modematched to the OPO cavity and generates a second (reference) blue beam in a direction opposite to the usual blue pump beam. This reference blue beam provides a faithful representation of the OPO cavity mode and is itself then modematched to the TEM_{00} mode of the transfer cavity C3 (but in a counter-circulating direction). With both the pump beam from the doubling cavity C2 and the reference beam from the OPO cavity efficiently matched to C3, we are ensured that the pump beam is in turn spatially matched to the OPO waist. The injected IR beam which generates the reference beam is then blocked as are the mirrors of C3, which consequently no longer acts as a resonant cavity but instead directly passes the pump beam from the doubling cavity (with a small loss of 2% introduced by the beam splitter which otherwise serves as the input coupler to C3).

For cw operation, the OPO cavity length is locked relative to the primary laser frequency ω so that a TEM_{00} longitudinal mode is resonant with the degenerate downconverted photons generated by the blue pump at frequency 2ω. In order to avoid interference of the locking light with the squeezed-vacuum field, the cavity length is locked by employing a counter-propagating and frequency-shifted locking beam LB, which is injected into the OPO cavity through M3 with an error signal derived in reflection at detector D_B as shown in Fig. 1. The frequency shift $\delta\omega = -170\,\text{MHz}$ for the locking beam is provided by an acoustooptic modulator (AOM) and is chosen equal to the transverse-mode spacing of the cavity. The locking beam is intentionally misaligned to maximize the transmission of the TEM_{10} mode adjacent to the TEM_{00} mode. Hence, when the resonance condition for the frequency-shifted transverse mode is satisfied, the principal unshifted TEM_{00} mode is likewise on resonance for the downconverted field at ω. On the other hand, the locking beam LB is both counter-circulating in the OPO and frequency shifted by 170 MHz from the frequency of the degenerate squeezed field and therefore has no appreciable deleterious effects (Note that the conjugate idler field that might be generated at $-\delta\omega$ is not coincident with any resonant mode of the OPO cavity).

C *Light-Induced Absorption*

Unfortunately while studying the OPO with $KNbO_3$, we have discovered a nonlinear mechanism that substantially increases the IR losses above the level of the passive linear losses of the crystal [30]. This effect is observed at temperatures far away from the phasematching conditions and is independent of the direction of propagation of the blue beam relative to the IR beam (parallel or antiparallel), so that it cannot be explained in terms of phase-matched non-

linear frequency conversion. To explore this phenomenon further, we measure the transmission and reflection of an IR beam injected into the OPO as a function of the blue pump power passing through the $KNbO_3$ crystal (and mode matched to the IR shape). The cavity is scanned through resonance and intracavity losses are then calculated from (i) the measured peak transmission and (ii) the depth of the resonance dip in the intensity of the reflected light. The results for the light-induced losses calculated from the transmission and reflection measurements are presented in Fig. 2 (traces (i) and (ii)). To explain the discrepancy between the two curves, we assume that in addition to the light-induced absorption, the tightly focussed blue beam also forms a thermal lens in the crystal which leads to reduced modematching efficiency for the injected IR beam. Expanding the incident field E_{in} in terms of the cavity transverse modes U_{nm},

$$E_{in} = \sum_{n,m} \alpha_{nm} U_{nm}, \tag{6}$$

we have that the intensities of the transmitted (I_t) and reflected (I_r) fields are given by

$$I_t = \frac{4TT_3}{(T+L)^2}\,\alpha_{00}^2 \tag{7a}$$

$$I_r = I_{in} - \frac{4TL}{(T+L)^2}\,\alpha_{00}^2, \tag{7b}$$

where we assume that the TEM_{00} mode is resonant and that L is the total intracavity loss. In (7), the injected beam is taken to be incident through the coupler M_1 with transmission T. The field transmitted by the cavity to give the intensity I_t is detected as the output through a high reflector M_3 with transmission $T_3 \ll T$, while the field reflected by the cavity mirror M_1 results in the intensity I_r. Suppose that without the blue pump E_{in} is perfectly modematched to the TEM_{00} cavity mode ($\alpha_{00} = 1$), while in the presence of the blue beam $\alpha_{00} < 1$ due both to a thermal lens effect and to a nonlinear loss term which takes $L \to L(P_2) + L$. A self-consistent expression for light-induced absorption $L(P_2)$ can be derived from (7a, 7b) to give

$$L(P_2) = L\left[\frac{I_t}{\tilde{I}_t(P_2)}\,\frac{I_{in} - \tilde{I}_r(P_2)}{I_{in} - I_r}\right], \tag{8}$$

with $\tilde{I}_t$ and $\tilde{I}_r(P_2)$ as the transmitted and reflected intensities on resonance in the presence of the blue pump of power P_2. The losses calculated from (8) are also plotted in Fig. 2 (trace (iii)) and are seen to lie intermediate between the losses inferred from transmission (i) (from (7a) alone) and reflection (ii) (from (7b) alone), indicating the qualitative importance of thermal lensing (and consequent degradation of mode matching).

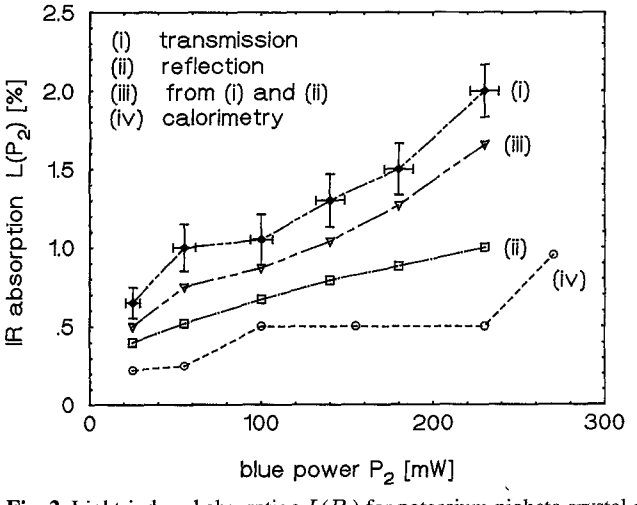

Fig. 2. Light-induced absorption $L(P_2)$ for potassium niobate crystal of length 10 mm vs power P_2 of the blue pump beam. The curves (i)–(iv) are calculated losses from measurements of (i) cavity transmission, (ii) cavity reflection, (iii) transmission and reflection self-consistently analyzed, and (iv) temperature rise in the presence of IR and blue beams. For $P_2 = 0$, the waist in the crystal for the IR beam is approximately 20 μm, while that of the blue beam is about 14 μm

An alternate confirmation of the existence of light-induced absorption is obtained from laser calorimetry measurements. A temperature sensor is placed on the copper housing which supports the crystal; the sensor is separated from the crystal by a 1 mm thick copper plate. The OPO cavity is illuminated by 110 mW of IR through mirror M1 to buildup a large field inside the resonator, which is itself locked to the laser frequency for cw operation. Under these conditions, the temperature change due to absorption of the circulating IR power through the crystal is $\delta T = 0.18°$ C. Next $\delta T(P_2)$ in the presence of the blue pump is measured, where $\delta T(P_2)$ is the temperature change exclusively due to IR absorption corrected for the temperature change due to simple absorption of the blue itself. Assuming the temperature change *at the sensor* is proportional to the increased bulk absorption at the IR wavelength, we find that the nonlinear loss is given by $L(P_2) = L_0[\delta T(P_2)/\delta T - 1]$, where the bulk crystal loss (exclusive of AR coatings) $L_0 = 0.2\%$ has been measured separately. The values of $L(P_2)$ vs P_2 determined in this fashion as also shown in Fig. 2 (curve (iv)), where it is clear that the results of calorimetry (iv) are substantially different from those calculated from transmission/reflection measurements (iii). Both the calorimetry and the transmission/reflection measurements have certain systematic errors, with the most obvious error for the calorimetry being that the temperatures are not measured directly in the crystal. While the measurements in Fig. 2 are for $\lambda = 847$ nm, we have also made measurements around 870 nm with no substantial difference in the results for the light-induced absorption. Note that the blue pump for these measurements is generated with a wavelength that is half the IR wavelength. Heating the crystal from 15° C to 60° C does not notably change the results in Fig. 2.

With regard to our squeezing experiment, the blue light induced losses degrade the efficiency with which squeezed fluctuations escape the cavity and are detected. Although the passive losses of our OPO cavity imply a loss-limited degree of squeezing $S_{ext} = -\varrho = -0.972(-15.6\,\text{dB})$, unfortunately we must generalize $\varrho \to \varrho(P_2) \equiv \dfrac{T}{T + L(P_2) + L}$. For 100 mW of blue pump focussed to a spot of waist $w_{bl} \cong 14\,\mu$m, we find for the actual squeezing measurements in the following section that $L(P_2) \cong 0.011$, and hence $\varrho(P_2) \cong 0.875$. Here we choose $L(P_2)$ as given by curve (i) in Fig. 2 from the transmission data, which roughly incorporates both the losses in efficiency due to absorption and

due to decreased modematching efficiency (which presumably impacts the homodyne efficiency). Although we are evaluating other crystals grown under a variety of conditions, the blue light induced IR absorption currently sets the major limitation on the degree of squeezing obtained in our experiment.

D *Observation of Frequency Tunable Squeezed Light*

Combining the results from the previous discussions, we obtain a simple theoretical expression for the expected degree of observed nonclassical noise reduction. Specifically, the ratio $R(\Omega,\theta_-) \equiv \Phi(\Omega,\theta_-)/\Phi_0$ is found from (3,4) to be

$$R(\Omega,\theta) = 1 - \xi\varrho\frac{4r^{1/2}}{[f^2+(1+r^{1/2})^2]}, \tag{9}$$

where $r = P_2/P_{20}$ is the dimensionless measure of the pump strength below threshold ($0 \le r < 1$) and $f \equiv \Omega/\Gamma$ is the dimensionless frequency offset in units of the cavity half-linewidth $\Gamma(P_2)/2\pi \equiv (c/l)[T + L(P_2) + L]/4\pi$ with l as the optical length of the cavity. The efficiency factor $\xi \equiv \zeta\alpha\eta^2 = 0.96$ with $\zeta = 0.98$ as the measured propagation efficiency, $\alpha = 1.00 \pm 0.02 \equiv 1.00$ as the measured quantum efficiency of the photodiodes (D1, D2) and $\eta = 0.99$ as the measured homodyne efficiency. Note that the LO beam passes through the mode cleaning cavity C4 to increase η (Fig. 1). The cavity C4 with 0.5 MHz linewidth (HWHM) also serves to reduce the excess amplitude noise of the LO at high frequencies. The spectral density of the photocurrent fluctuations $\Phi(\Omega,\theta)$ is measured at the frequency $\Omega/2\pi = 1.4$ MHz which is chosen to be high enough to be largely beyond the extreme technical noise of the Ti : Al_2O_3 laser but which is low enough not to lose too much squeezing because of the finite squeezing bandwidth. Since the losses $[L(P_2) + L]$ depend on the pump power P_2 because of the light-induced loss $L(P_2)$, there is some optimum level of P_2 corresponding to maximum squeezing. Having measured the functional dependence $L(P_2)$, we find that the optimum pumping power is about $P_2 \cong 100$ mW, so that $r \cong 0.4$ and $f \cong 0.25$. Substituting these various terms into (9), we find that $R(\theta_-) \cong 0.22(-6.6\,\text{dB})$. Note that the observed threshold power P_{20} is higher than that predicted by (5) because of the light-induced losses and the imperfect modematching of the pumping beam.

Although in the current experiment the OPO is operated below threshold, it is worth nothing that our OPO design is characterized by exceptional stability of operation above threshold. With the cavity length of the OPO stabilized as described in Sect. 1.2, we have obtained 100 mW of stable cw down-converted radiation for above threshold operation with 250 mW of blue pump in a cavity with output coupler M_1 of transmission $T = 0.05$. The estimate based on (5) shows that we can expect the threshold of $\sim$ 1 mW for $T \sim 0.5\%$.

To observe squeezed-state generation for operation below threshold, we record the spectral density of photocurrent fluctuations $\Phi(\Omega,\theta)$ for the photocurrent i_- for fixed RF analysis frequency Ω and varying phase θ (proportional to time) between the local oscillator beam from cavity C4 and the squeezed-vacuum field from the OPO (Fig. 1). Figure 3 displays a trace obtained in this fashion (trace (i)) with phase-sensitive fluctuations both above and below the vacuum-state level Φ_0 (trace (ii)). Also shown in the figure is a trace (iii) taken with the phase offset between the local oscillator and the squeezed beam actively servo controlled for minimum photocurrent fluctuations ($\theta = \theta_-$). For these measurements, Φ_0 is determined with an accuracy of $\pm$ 0.2 dB, with the uncertainty largely due to drifts of the dc power level of the (unstabilized) local oscillator. The amplitude noise spectrum of the local oscillator field for a power level of 0.5 mW at either detector (D1, D2) has excess noise above the coherent-state limit of about 9 dB for $\Omega/2\pi = 1.4$ MHz. The balanced homodyne detector suppresses this excess noise by about 34 dB. The directly observed noise level (iii) in Fig. 3 lies $-(6.0\pm0.3)$ dB below the vacuum-state limit set by Φ_0 corresponding to a nonclassical noise level $R(\theta_-) = 0.25 < 1$. This result is in reasonable agreement with our theoretical estimate of $R(\theta_-) = 0.22$. The level Ψ_0 lies 20 dB above the thermal noise level of the photodetector electronics [36].

An important point to note is that squeezing traces such as presented in Fig. 3 remain unchanged as the reference cavity C1 (and hence the laser frequency and the doubling-cavity resonance and the OPO output field) is scanned continuously over a range of 2 GHz, making this source practical for spectroscopic applications. With the entire system locked in this fashion, stable cw squeezing can be generated in an uninterrupted fashion for long intervals ($\sim$ 1 h).

2 Atomic Spectroscopy with Squeezed Light

A *Theoretical Background*

The source of squeezed light described in the previous section provides substantial quantum noise reduction in the spectral components of the photocurrent around 1.4–3.0 MHz. This frequency interval is chosen since it is close to the optimum for the modulation frequency of $\Omega_0/2\pi \sim 5$ MHz in FM spectroscopy of the $D2$ line of Cs (of linewidth 5 MHz (FWHM)); the resonant response of our tuned photodetector electronics has been optimized here. As a consequence of the nonclassical noise reduction, a spectroscopic signal encoded in this frequency region should be detectable with sensitivity below the usual shot-noise limit. However, before addressing this issue, let us first describe the conventional spectroscopic method of FM saturation spectroscopy which is known to be capable of providing shot-noise limited spectroscopic signals [15–17]. A broad outline of this technique is shown in Fig. 4a, where a probe beam passes through an electrooptic modulator (EOM) to yield a frequency modulated field $E_p = A_0 \exp[-i(\omega t + \beta\sin\Omega_0 t)] + \text{c.c.}$, where β is the modulation index for the sinusoidual modulation at Ω_0 and $|A_0|^2 \sim$ photons/s. This field is shown in a phasor diagram in Fig. 4b(i) where the rotating frame is that of the carrier at frequency ω. The field components $E_\pm$ (with $|E_\pm| = \beta A_0/2$) are shifted from the carrier by $\pm\Omega_0$ and hence rotate in opposite directions to yield a sum field E orthogonal to the carrier A_0 [pure frequency modulation (FM)]. If there is no frequency selective

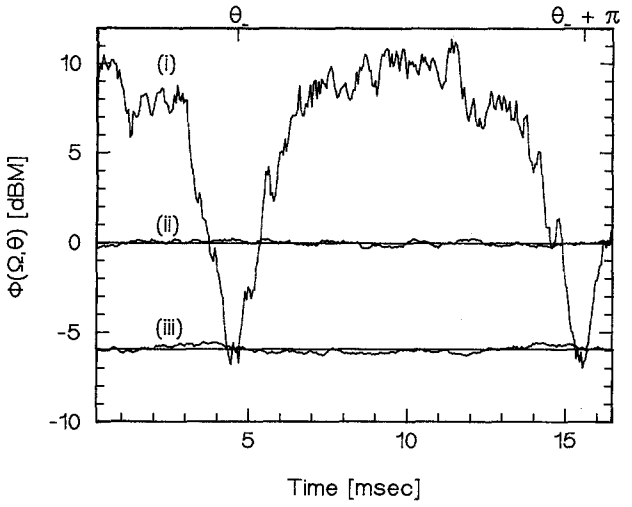

Fig. 3. Spectral density $\Phi(\Omega, \theta)$ for the fluctuations of the photocurrent i_- (Fig. 1). Trace (i) is for a squeezed-vacuum input to the balanced detector with the local oscillator phase θ swept with a linear ramp. Trace (ii) is a ten-trace for a vacuum-state input and sets the "shot-noise" level. Trace (iii) is likewise an average of ten traces, but is acquired with a squeezed-vacuum input with the phase θ actively controlled for minimum photocurrent fluctuations (That is, $\theta \cong \theta_-$ for this trace). Acquisition parameters are $\Omega/2\pi = 1.4$ MHz detection bandwidth = 100 kHz, video bandwidth = 1 kHz, (trace (i)), = 100 Hz (traces (ii) and (iii)), sweep time for trace (i) = 15 ms, local oscillator power = 0.5 mW, wavelength = 856 nm

absorption/dispersion in the path of the probe beam as in Fig. 4b(ii) (or no imbalance from the intervening medium), a square-law detector produces zero modulation in the photocurrent at Ω_0 because E_p remains a field with FM only. However, a narrow atomic resonance can introduce differential absorption/dispersion between the sidebands and the carrier, thus converting a fraction of the FM field into an AM field, which is then detected to produce a modulated photocurrent at Ω_0. This effect is illustrated in Fig. 4b(iii), where the result of a frequency-selective response for the medium is to make the sum of E_+ and E_- no longer orthogonal to A_0, so that there arises a component of amplitude modulation. As illustrated in Fig. 4b(iv), the detected modulation in the photocurrent at frequency Ω_0 depends upon the detuning of the carrier frequency ω from the atomic resonance ω_0.

For a more quantitative analysis we employ the theory of [16] to calculate the spectroscopic signal for the case of both probe and pump beams as coherent-state fields. In the limit of small modulation index ($\beta \ll 1$), the electric field of the probe beam emerging from the EOM is

$$E_p = A_0\{\exp(-i\omega t) - \frac{\beta}{2}\exp[-i(\omega - \Omega_0)t] + \frac{\beta}{2}\exp[-i(\omega + \Omega_0)t]\} + \text{c.c.}. \quad (10)$$

Assuming an atomic vapor which is optically thin, the transmission factors for the carrier and the sidebands $t(\omega) = \sqrt{T_0}\exp(-i\phi_0)$ and $t_\pm(\omega) = \sqrt{T_0}\exp[-(\delta_\pm + i\phi_\pm)]$ can be expanded to first order to yield a mean signal photocurrent given by

$$\langle i_s(t)\rangle = e\alpha|A_0|^2T_0[1 + (\delta_- - \delta_+)\beta\cos\Omega_0 t + (\phi_+ + \phi_- - 2\phi_0)\beta\sin\Omega_0 t], \quad (11)$$

with α as the quantum efficiency of the photodetector D for the probe beam (Fig. 4a). The rms signal photocurrent measured by a (phase insensitive) spectrum analyzer around the modulation frequency Ω_0 is then

$$i_s(\Omega_0) = e\alpha\beta|A_0|^2T_0[(\delta_+ - \delta_-)^2 + (\phi_+ + \phi_- - 2\phi_0)^2]^{1/2}/\sqrt{2} \equiv e\alpha\beta|A_0|^2T_0\Delta/\sqrt{2}, \quad (12)$$

where the last equality defines the atomic response function Δ, which of course depends on the detuning of the carrier frequency ω relative to the atomic resonance ω_0 through the dependence of the factors $[\delta_\pm, \phi_\pm, \phi_0]$ on $(\omega - \omega_0)$. Note that we assume throughout detection of the modulus of the atomic response Δ rather than of the individual RF quadratures for absorption ($\cos\Omega_0 t$) and dispersion ($\sin\Omega_0 t$).

As pointed out in [16], a complete density matrix description for the frequency dependence of (δ, ϕ) in saturation spectroscopy is quite complex [31]. A much simpler rate equation approach yields qualitatively similar results

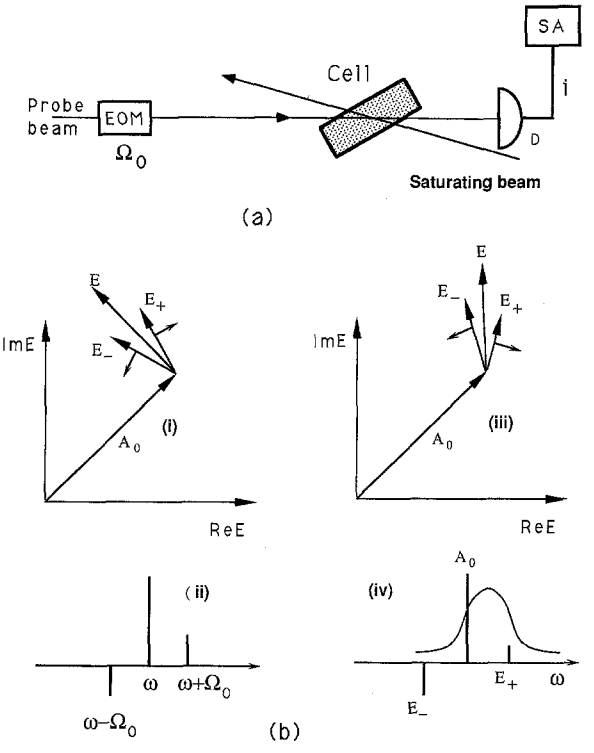

Fig. 4a, b. Outline of FM saturation spectroscopy method. **a** A probe beam is frequency modulated by the electrooptic modulator (EOM) and passes through a cell filled with atomic vapor and excited by a strong counterpropagating saturating beam. The spectral density $\Psi(\Omega_0)$ of the resulting photocurrent i around the modulation frequency Ω_0 is measured by a spectrum analyzer (SA). **b** (i) A phasor diagram at the carrier frequency ω shows frequency sidebands E_+ and E_- frequency shifted with respect to the coherent carrier amplitude A_0 by $\pm\Omega_0$. $E_\pm$ are generated when the probe beam passes through the EOM and sum to give the modulation field E. (ii) Prior to passing through the cell, E is shifted in phase by 90° with regard to the carrier (pure FM sidebands). (iii) The narrow saturated atomic resonance causes differential absorption/dispersion of E_+ and E_- resulting in an imbalance of $E_\pm$ and in a phase shift of the modulation field E. (iv) FM is partially converted into AM to produce a coherent modulation at Ω_0 in the photocurrent at D

that will suffice for our present purposes. We proceed by first writing $\delta = \delta_L + \delta_{NL}$ as a sum of a linear Doppler background term δ_L and of a nonlinear term δ_{NL} due to effects of a counter-propagating saturating beam. Here δ_L is given by [16]

$$\delta_L(\omega) = \frac{\alpha_p d}{2}(1+S_p)^{-1/2}\exp\left[-\left(\frac{\omega-\omega_0}{ku}\right)^2\right], \tag{13}$$

with S_p as the saturation parameter for the probe beam, ku as the Doppler width (with $k \equiv \omega/c$ and u as the mean thermal speed), d as the sample length, and α_p as the peak absorption coefficient. δ also includes a narrow saturated resonance described by δ_{NL} which emerges from a velocity resolved peak in the excited state population. As in [16], we find

$$\delta_{NL}(\omega) = -\frac{\alpha_p d}{8}\exp\left[-\left(\frac{\omega-\omega_0}{ku}\right)^2\right] \times \frac{\left(\frac{\sqrt{1+S_p}+\sqrt{1+S_s}}{\sqrt{1+S_p}\sqrt{1+S_s}}\right)S_s}{\left[\left(\frac{\sqrt{1+S_p}+\sqrt{1+S_s}}{2}\right)^2+(\omega-\omega_0)^2T_2^2\right]}, \tag{14}$$

with S_s as the saturation parameter for the saturating beam and T_2 as the transverse relaxation time for the atomic medium. For the simple case of a single two-state transition, δ_L and δ_{NL} are centered about the same frequency ω_0. However, for the particular case of the $6^2S_{1/2} \rightarrow 6^2P_{3/2}$ transition in atomic cesium ($D2$ line at 852 nm) that we employ, there are a variety of hyperfine transitions that sum with different transition frequencies and weights to produce the actual Doppler-broadened linear absorption profile $\delta_L(\omega)$. Distributed across this profile are the narrow-Doppler free resonances, whose actual form can depend sensitively on factors such as the relative polarizations of pump and probe beams. For maximum simplicity and clarity in our proof-of-principle experiment, we will concentrate on the $F = 4 \rightarrow F' = 5$ transition of the $D2$ line, which is close to the center of the Doppler profile.

In a fashion similar to the derivation leading to (13) and (14) for (δ_L, δ_{NL}), one can derive expressions for the dependence of the phase ϕ on laser frequency ω. The nonlinear part of the dispersive response is found to be [16]

$$\phi_{NL}(\omega) = \frac{\alpha_p d}{4}\exp\left[-\left(\frac{\omega-\omega_0}{ku}\right)^2\right] \times \frac{\frac{S_s}{\sqrt{1+S_s}}(\omega-\omega_0)T_2}{\left[\left(\frac{\sqrt{1+S_s}+\sqrt{1+S_p}}{2}\right)^2+(\omega-\omega_0)^2T_2^2\right]}. \tag{15}$$

Upon substituting (15) and (14) into (12), we find the signal photocurrent $i_s(\Omega_0)$ vs ω which (as we will see) has a characteristic "M"-shape as a function of the carrier frequency ω of the probe beam [16, 17].

Calculation of the saturation parameter $S \equiv I/I_0$ for a multilevel system is not a trivial problem. For a two-state system the saturation intensity I_0 is determined by the following expression:

$$I_0 = \frac{\hbar\omega_0}{2\sigma\tau}, \tag{16}$$

with $\sigma \equiv \frac{3}{2\pi}\lambda^2$ as the absorption cross-section and τ as the excited state lifetime. In the case of the D2 line of cesium, each hyperfine transition is degenerate with regard to magnetic quantum number, so that I_0 is polarization dependent. The process of optical pumping makes the issue of the calculation of I_0 even more complex. The ratio $S_s/S_p = \frac{P_s}{P_p}\frac{w_p^2}{w_s^2}$ is known from the experiment with P as the power and ω as the waist of the probe (p) and saturation (s) beams. With this ratio fixed, we treat I_0 as a free parameter in our least square fitting of the experimental spectroscopic traces. The value of I_0 that we find from this procedure is about 1.7 mW/cm^2, which is in qualitative agreement with the value 1.04 mW/cm^2 that one obtains from (16). Other free parameters in our fits to the FM spectra are the peak absorption $\alpha_p d$ and an additive constant emerging from approximating the broad linear contribution of the Doppler background to δ_L and ϕ_L as a simple offset.

For spectroscopy with the probe beam in a coherent state, the noise against which the signal photocurrent $i_s(\Omega)$ must be detected is given by the shot-noise photocurrent [14–17, 21]

$$i_n^2 = 2e^2\alpha T_0|A_0|^2B, \tag{17}$$

with B as the detection bandwidth. From (12) and (17) we thus arrive at a signal-to-noise ratio for measurements limited by the vacuum fluctuations of a coherent state given by

$$Q_v \equiv \frac{i_s^2}{i_n^2} = N\Delta^2/2, \tag{18}$$

where $N = \alpha T_0\beta^2|A_0|^2/2B$ is the number of photoelectrons generated in a time B^{-1} as a result of the photon flux for the FM sidebands of the probe beam. For $Q_v = 1$, the minimum detectable atomic response is then $\Delta_v = 2/\sqrt{N}$, which is the usual quantum limit set by the vacuum fluctuations of the field. Note that the factor $\sqrt{2}$ appears because we have assumed phase insensitive detection of the two RF quadratures at Ω_0.

If we next consider the case of a squeezed probe field with $|A_0|^2 \gg \int d\Omega S(\Omega,\theta_+)$ (i.e., small squeezed fluctuations as compared to the energy of the mean field), then the principal effect associated with the presence of squeezing is the alteration of the noise current from i_n^2 to a value $i_{sq}^2(\Omega_0,\theta) = i_n^2[1+\xi'\varrho S(\Omega_0,\theta)]$, where $\xi' = T_0\xi$ [14, 21]. Since i_s is unchanged in this limit (with again $\beta \ll 1$), the signal-to-noise ratio becomes $Q_{sq} = Q_v[1+\xi'\varrho S(\Omega_0,\theta)]^{-1}$, with corresponding minimum detectable response $\Delta_{sq} = \Delta_v[1+\xi'\varrho S(\Omega_0,\theta)]^{1/2}$. For efficient propagation and detection with $\xi' \rightarrow T_0 \cong 1$ and for large squeezing with

$\varrho S(\Omega_0, \theta_-) \to -1$, there is thus an enhancement E in signal-to-noise ratio

$$E \equiv \frac{Q_{sq}(\theta_-)}{Q_v} \sim (1 - T_0)^{-1} \gg 1, \tag{19}$$

and a reduction in the minimum detectable response $\Delta_{sq}(\theta_-)/\Delta_v \sim (1 - T_0)^{1/2} \ll 1$. In our experiment $1 + \xi' \varrho S_- \cong 0.35$. Hence we might expect an enhancement in signal-to-noise ratio $E \cong 3.0(4.6\,\text{dB})$ and a reduction of the minimum detectable response to $\frac{\Delta_{sq}(\theta_-)}{\Delta_v} \cong 0.6$.

Although our discussion assumes that the improvements in sensitivity are limited by the system losses, there will of course be a limit imposed in principle as the degree of squeezing becomes large ($|A_0|^2 \sim \int d\Omega S(\Omega, \theta_+)$). Precisely as in the classic work of Caves [33], a maximum enhancement in sensitivity will be reached when the fluctuations from the noisy unsqueezed quadrature begin to contaminate the measurement of the quiet quadrature (assuming of course that the system has sufficiently low losses). However, even in the loss-limited case, new behavior can emerge since the noise floor will not be constant as the laser frequency ω is swept, but instead will itself be a function of laser detuning as the losses (and hence the degree of detectable squeezing) and the phase shifts (and hence the observed squeezing quadrature) vary across the atomic profile.

B *Squeezed-Light Spectroscopy Experiment*

The experimental setup for employing squeezed light in atomic saturation spectroscopy is shown in Fig. 5. A beam in a squeezed-vacuum state is generated by the OPO as described in Sect. 1. A fraction of the local oscillator beam emerging from the cavity C4 (Fig. 1) now serves as the probe beam. The squeezed vacuum is combined with the coherent probe beam at the mirror M2 in Fig. 5; the reflectivity for the squeezed beam is 98.5%. The degree of squeezing is of course degraded by the additional 1.5% loss; however, this is of small consequence given the other losses in the current setup. If the probe beam is shot-noise limited around the frequency Ω_0 of interest, then the quantum-noise reduction for the photocurrent i of the single detector D in Fig. 5 is again described by (4), where now θ refers to the phase angle between the coherent amplitude of the probe beam and the axis of the squeezing ellipse for the field from the OPO and where we denote Ψ as the spectral density for the photocurrent i. We should emphasize that although there is a loss of probe power at M2 due to its high reflectivity, there is not a corresponding degradation in signal-to-noise ratio for FM spectroscopy since in fact atomic saturation is the ultimate arbitrator for the allowed intensity (and hence power for a given beam waist) for the probe beam.

With the squeezed-vacuum beam blocked, the setup shown in Fig. 5 is the usual setup for "classical" FM spectroscopy [15–17, 32]. The electrooptic modulation (EOM) provides frequency modulation of the probe beam at $\Omega_0/2\pi = 2.7\,\text{MHz}$. The polarizers (P1, P2) in the figure are used to decouple the probe and saturating beams, which have orthogonal polarizations. An acoustooptic modulator (AOM) is placed in the saturating beam and shifts its frequency by $-40\,\text{MHz}$ to eliminate interference between the probe beam and scattering from the saturating beam. The laser is tuned to a wavelength of 852.36 nm corresponding to the $6S_{1/2} \to 6P_{3/2}$ line of atomic Cs. As previously mentioned, we focus attention on the particular hyperfine transition $F = 4 \to F' = 5$ (insert in Fig. 5). Minimization of residual AM [34, 35] is facilitated with polarizer P2 as well as by very careful alignment and large detection bandwidth. The reference cavity C1 (Fig. 1) which determines the frequency for the titanium-sapphire laser (and hence for the entire setup) is scanned around the $4 \to 5$ resonance by way of a PZT mounted mirror. The analysis frequency of the spectrum analyzer coincides with the coherent modulation frequency Ω_0. In order to use a more powerful probe beam to overcome electronics noise in the detectors while at the same time avoiding oversaturation of the atomic medium, the probe beam is expanded by a telescope to have a waist of 1.5 mm. The saturating beam has a waist of 3.2 mm (and a total power of 1.5 mW) and is aligned antiparallel to the probe beam. The power of the probe beam after transmission through the reflector M2 is 130 μW and is chosen to be as high as possible for best sensitivity consistent with "reasonable" lineshapes of the form described by (14, 15).

Turning to the spectroscopy results, we first display in Fig. 6 the spectral density $\Psi(\Omega_0)$ for the photocurrent i (Fig. 5) vs laser detuning $\nu \equiv \omega/2\pi$. The FM spectroscopic signal is taken for a coherent probe with high optical den-

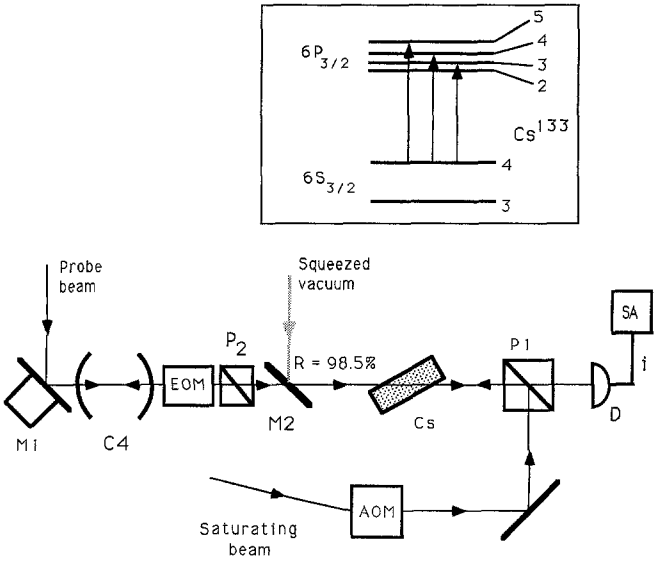

Fig. 5. Experimental setup for FM spectroscopy with squeezed light. The entire setup is basically the same as in Fig. 1 with the exception of the part shown here. The 50/50 beamsplitter for the balanced homodyne detector in Fig. 1 is replaced by a mirror M2 with reflectivity $R = 98.5\%$. The local oscillator shown in Fig. 1 now serves as a probe beam and has FM sidebands encoded with the EOM. The probe beam is combined with the squeezed-vacuum field from the OPO at M2 and then passes through a cesium cell at Brewster angle with an absorption path length of 17 mm. A counterpropagating and orthogonally polarized saturating beam is frequency shifted by $-40\,\text{MHz}$ with respect to the probe frequency. Coherent modulation at Ω_0 (the "signal") as well as the quantum fluctuations of the probe beam (the "noise") are detected at D, appear in the photocurrent i, and are analyzed by the spectrum analyzer (SA) to determine the spectral density $\Psi(\Omega_0)$

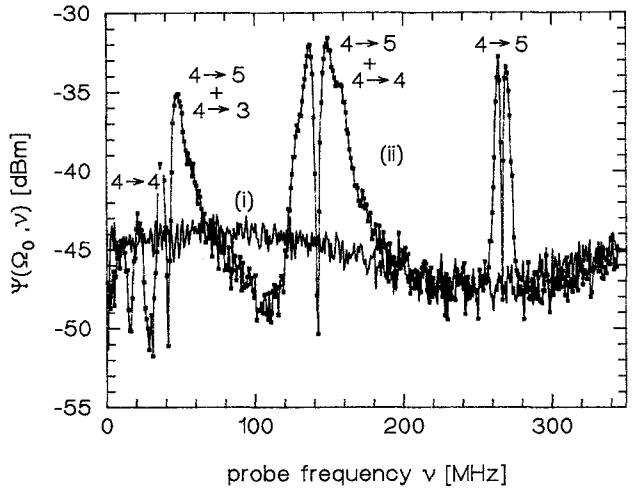

Fig. 6. Spectral density $\Psi(\Omega_0)$ vs probe frequency $\nu \equiv \omega/2\pi$ for the case of a coherent-state probe beam. These traces are taken for high optical density and illustrate (i) the linear Doppler background obtained with saturating beam blocked and (ii) the FM saturation spectroscopy signal in the presence of the saturating beam. The various sub-Doppler resonance features are labeled with reference to the hyperfine components of the ground and excited states of the D_2 line of atomic cesium

sity of Cs vapor to demonstrate the characteristic features of the spectrum with high signal-to-noise ratio. Trace (i) represents the linear Doppler signal at Ω_0 obtained with the saturation beam blocked. With the saturation beam present (trace ii), each resonance in the atomic response produces a narrow, roughly "M"-shape feature in the FM spectroscopy signal (see below). In fact, trace (i) is the central part of the broad "M" corresponding to the broad Doppler profile centered around 260 MHz on the horizontal axis (the frequency origin for the scan is arbitrary). In trace (ii) each of the hyperfine transitions $4 \rightarrow 5$, $4 \rightarrow 4$ and $4 \rightarrow 3$ produces a narrow feature (only $4 \rightarrow 4$ and $4 \rightarrow 5$ are shown in Fig. 6). Additionally, there are crossover resonances situated half the distance between each pair of the hyperfine resonances [32]. The reason that the narrow Doppler-free resonances (except for the $4 \rightarrow 5$ transition) are so asymmetric is that there is appreciable interference from the Doppler background. The $4 \rightarrow 5$ resonance is reasonable symmetric because it lies closest to the central minimum of the Doppler profile; in fact, the sign of the 40 MHz frequency shift of the saturation beam has been chosen for this very reason.

After these measurements with relatively high cesium density ($3 \times 10^{10}/\text{cm}^3$) are completed, the Cs cell is next cooled from room temperature down to about 0° C to pass to a regime of small signal-to-noise ratio for coherent-state FM spectroscopy. We concentrate on the $4 \rightarrow 5$ transition and decrease the scanning range to 50 MHz. The resulting FM spectrum with the squeezed-vacuum input to mirror M2 in Fig. 5 blocked is shown in Fig. 7a, where the solid curve is from the sum $[i_s^2(12, 14, 15) + i_n^2(17)]$ with the center frequency chosen for best fit and a small offset added to account for the Doppler background. This theory is not quantitatively correct for our measurements since it is developed for a two-state atom with $\Omega_0 \gg 1/T_2$ in a rate-equation approximation. However, the qualitative character of the lineshapes is nonetheless sufficient for our discussion (as indicated by the quality of the fit in the figure) especially since the domain

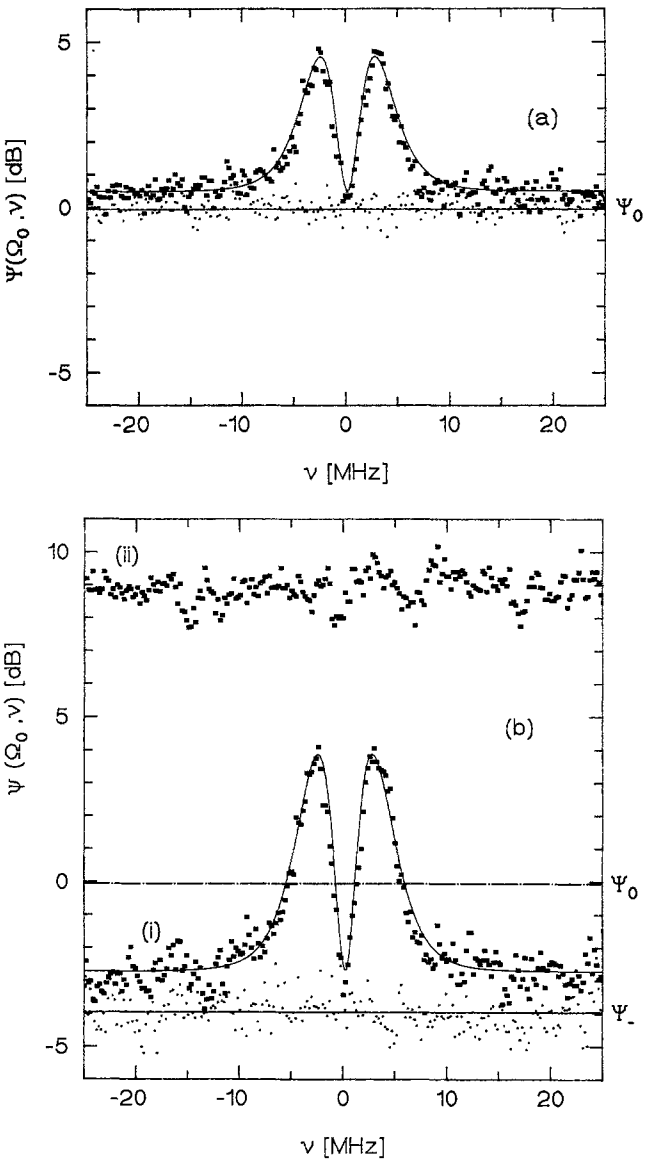

Fig. 7a,b. Spectral density $\Psi(\Omega_0, v)$ for the probe photocurrent i at Ω_0 vs laser frequency $\nu \equiv \omega/2\pi$ in the absence and presence of squeezed light. **a** Squeezed beam E_s blocked to illustrate the usual vacuum-state limit for FM spectroscopy. The points • are taken with $\beta = 0$ (no modulation) and set the shot-noise level Ψ_0, while the points ■ are acquired with $\beta = 0.02$ and give the level of signal plus noise. **b** Squeezed beam present demonstrating both an enhancement (i) and a degradation (ii) in sensitivity relative to the usual quantum limit. Points • are taken with $\beta = 0$ at the noise minimum Ψ_-, while points ■ are taken with $\beta = 0.02$ with the phase between the probe and the squeezed field adjusted for minimum (i) and maximum (ii) photocurrent fluctuations. In (a-b) the thermal noise of the detector (which is 8.5 dB smaller than the "shot-noise") has been subtracted to yield the points displayed. The full curves are form the theory of [16] as discussed in the text. Acquisition parameters are $\Omega_0/2\pi = 2.7$ MHz, resolution bandwith = 300 kHz, video bandwidth = 300 Hz, sweep time = 0.2 s

of interest is one of low signal-to-noise ratio. For the traces in Fig. 7, the residual AM lies 24 dB below the shot-noise level. The small pedestal evident in the figure that raises the narrow signal above the shot-noise level (which is obtained with the FM turned off, $\beta = 0$) is attributed to the broad Doppler background with only a smaller contribution (~ 0.02 dB) arising from residual AM.

Our results for spectroscopy with squeezed light are obtained with the squeezed-vacuum input to mirror M2 in Fig. 5 unblocked. As shown in Fig. 7b trace (i), the phase offset for the squeezing relative to the mean probe amplitude can be set to minimize the quantum noise (amplitude-squeezed probe), with a resulting enhancement in the signal-to-noise ratio for detection of the atomic response $\Delta(\omega)$. On the other hand in trace (ii), the phase is adjusted to maximize the quantum noise (phase-squeezed probe), with a resulting rise in noise of about 9 dB above the shot-noise level to obliterate completely the spectroscopic signal. The theoretical curve in Fig. 7b for the data trace (i) is drawn with the same parameters as in Fig. 7a, except that the noise level is reduced by the observed drop of 3.8 dB (Ψ_0 is the shot-noise level in the figure; Ψ_- is the noise level with no FM sidebands $\beta = 0$). We should note that the problem of maintaining the optimum phase between the probe field and the squeezed vacuum from the OPO is complicated in a spectroscopy experiment by the fact that the frequency of the laser is being scanned, with the phase change $\delta\theta$ between the beams given by $\delta\theta = \delta\omega(l_{LO} - l_{SV})/e$, where the laser frequency is tuned by $\delta\omega$ and $(l_{LO} - l_{SV})$ is the optical path difference between the two beams. The path length l_{SV} for the squeezed vacuum includes the phase compounded by the frequency-doubled beam at 2ω as well as that from the OPO cavity. For a laser frequency scan of $\delta\omega = 50$ MHz along the abscissa in Fig. 7, the differential phase $\delta\theta$ across the scan is about 10 rad for our setup. As a result of this phase change, the spectroscopy signal observed should have a noise level which changes as $\cos^2(\delta\theta)$ along the scan, much as in Fig. 3. To eliminate this variation of the noise with $\delta\omega$ the photocurrent fluctuations from detector D are sampled at an auxilliary RF frequency of 3 MHz. By applying a small phase dither to the LO beam, an error signal suitable for the active stabilization of the phase offset between the local oscillator and squeezed fields can be obtained upon lock-in detection at the dither frequency. The results shown in Fig. 7b are acquired with the phase offset actively stabilized for either minimum (trace (i)) or maximum (trace (ii)) photocurrent fluctuations at 3 MHz. As previously mentioned, the frequency origin for the sweeps in Fig. 7 is arbitrary being referenced only to the length of the reference cavity, which is not actively stabilized to an absolute standard.

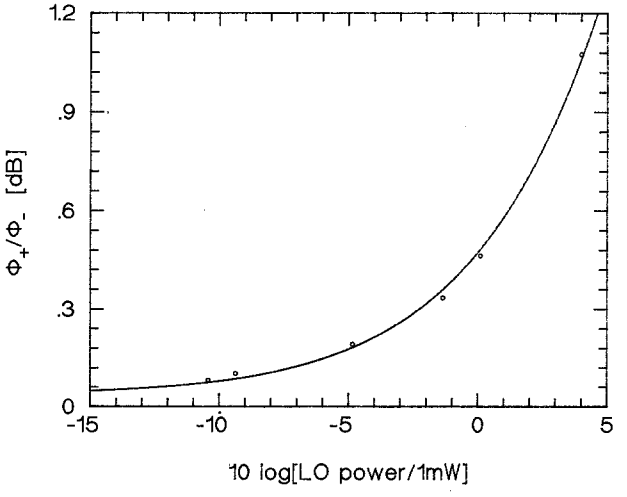

Fig. 8. Ratio of noise levels $\Phi_+(\Omega_0)/\Phi_-(\Omega_0)$ for the balanced detector of Fig. 1 versus local oscillator power for $\Omega_0/2\pi = 2.7$ MHz (with a vacuum-state input to the signal port). In the absence of excess technical noise (i.e., for a coherent state), $\Phi_+/\Phi_- = 1$ independent of power. The full curve is a fit to the data (with detector thermal noise subtracted) which includes a quadratic dependence in local oscillator power for the excess noise in Φ_+ and an offset of 0.04 dB to account for small imbalances in the circuits for summing and differing of $i_{1,2}$

The results shown in Fig. 7b taken with squeezed light indicate a quantum noise reduction of about $[3.8 \pm 0.2]$ dB and a corresponding enhancement of the signal-to-noise ratio. These data have had the thermal noise of the detector (which lies 8.5 dB below the shot-noise level) subtracted; before subtraction, the directly observed noise level for the squeezing trace with $\beta = 0$ lies 3.1 dB below the combined level of amplifier and shot noise [36]. The principal reason for the smaller quantum-noise reduction obtained in Fig. 7 as compared with the result shown in Fig. 3 is that the detection efficiency is decreased down to about 0.7 due to additional losses from the beam splitter, lenses, Cs cell, and polarizer P1. Note that in addition to enhanced sensitivity for the narrow Doppler-free signal in moving from Fig. 7a to 7b (trace (i)), the broad contribution to the signal spectrum associated with the Doppler background is also more discernible.

Because of the large technical noise of our Ti:Al_2O_3 laser (especially around 700 kHz due to relaxation-oscillation), it is important to ensure that the noise level Ψ_0 quoted in connection with Fig. 7 is the true "shot-noise" level. Toward this end, we have characterized the noise spectrum of the Ti:Al_2O_3 laser and present in Fig. 8 one result from this work. Shown in the figure is the ratio of noise levels Φ_+/Φ_- from the balanced homodyne detector in Figure 1 as a function of local oscillator power (we have also replaced the single detector D in Fig. 5 with a balanced detector arrangement to determine excess noise with results consistent to those quoted below). For a LO beam with no excess noise and with a vacuum-state input to the signal port of the balanced detector, the ratio $\Phi_+(\Omega_0)/\Phi_-(\Omega_0) = 1$, where $\Phi_+(\Phi_-)$ is the spectral density for photocurrents, $i_{1,2}$ summed in phase (with 180° phase shift). From Fig. 8 it is clear that excess technical noise which is masked at low power levels emerges with increasing power. The asymptotic value of Φ_+/Φ_- for zero local oscillator power should be 1; the offset of 0.04 dB is presumably due to a lack of identical characteristics for the $(\pm)$ configurations. Independent measurements of the electrical characteristics for the two configurations leads to an imbalance of $[0.00 \pm 0.05]$ dB (as indicated by the choise of the ordinate in Fig. 8). At the power level and RF frequency appropriate to the measurements of Fig. 7, we infer from Fig. 8 that the probe beam has excess technical noise of about 0.05 dB, which is considerably smaller than the other uncertainties for these data, but which is nonetheless incorporated into the indicated level for Φ_0 in Fig. 7.

For the data presented in Fig. 7, the modulation index $\beta = 0.02$. Of course the sensitivity in FM spectroscopy depends strongly on β and reaches a maximum for $\beta \cong 0.3$ [16, 17]. However, our measurements show that for $\beta > 0.02$, the observed quantum-noise reduction is degraded, as is illustrated in Fig. 9. Displayed in the figure are two squeezing traces taken with the spectroscopy setup of Fig. 5, but with the laser detuned from the atomic resonance. Curve (ii) is taken with modulation index $\beta = 0.1$ and clearly shows less

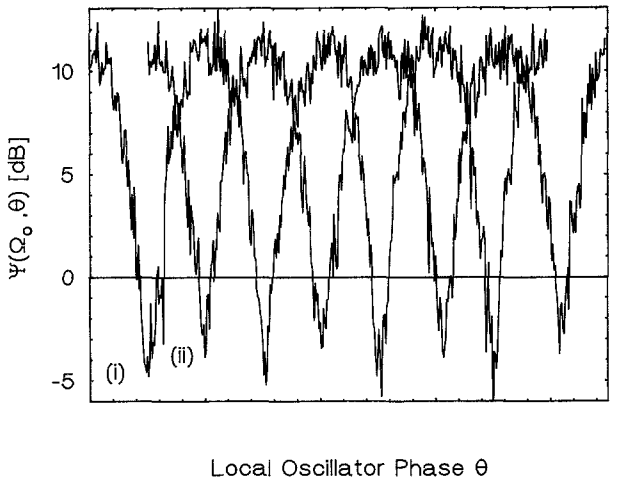

Fig. 9. Degradation of quantum-noise reduction due to increased FM modulation index for the coherent probe beam. Spectral density $\Psi(\Omega_0)$ of the photocurrent noise around 2.5 MHz vs the phase of squeezing for (i) FM off, (ii) FM on with modulation index $\beta = 0.1$. The probe frequency is detuned from the atomic resonance. Acquisition parameters are detection bandwith = 300 kHz, video bandwith = 3 kHz, sweep time = 100 ms

quantum-noise reduction than for curve (i) which is taken with the FM modulation off ($\beta = 0$). A similar trace with $\beta = 0.05$ shows less that 0.5 dB degradation for the minimum noise level. The degradation of squeezing for larger β is the subject of continuing investigation and is presumably associated with heterodyne noise which arises from mixing of the coherent FM sidebands with the squeezed fluctuations of the conjugate (noisy) quadrature [37].

3 Summary and Conclusions

We have described a cw frequency tunable source of squeezed light for spectroscopic applications and have demonstrated a directly observed nonclassical reduction in photocurrent fluctuations 6.0 dB below the vacuum-state level. The implementation of this source in FM saturation spectroscopy of atomic cesium has resulted in a directly observed improvement of measurement sensitivity of 3.1 dB beyond the usual quantum limit. After correction for electronics noise, the level of improvement increases to 3.8 dB. Because of the potentially broad tunability of our source over the 90° C phase-matching bandwidth of $KNbO_3$ (840-970 nm), enhanced detection sensitivity should be readily attainable for atoms and molecules other than Cs and could lead to improved capabilities in a variety of spectroscopic investigations which are currently shot-noise limited. Of particular relevance are applications involving transient species (as in reaction kinetics) and weak absorption lines (as in overtone spectroscopy) where the measurement time or power is restricted.

Beyond the demonstration of proof-of-principle feasibility for the use of squeezed light in atomic spectroscopy, there are a number of ways to improve these initial results. Eliminating the different sources of dissipation (especially the light-induced absorption in the crystal) is a straightforward avenue to follow to increase the quantum-noise reduction. Indeed, without the process of light-induced absorption, the passive escape efficiency ϱ would correspond to a loss-limited degree of squeezing 16 dB below the vacuum level for the output field of the OPO, with the various other efficiency factors then leading to a subsequent loss-limited reduction of 11 dB for the observed photocurrent fluctuations. Apart from improved efficiencies, there is also a need to increase the cavity bandwidth Γ to increase the sensitivity in FM spectroscopy by allowing larger values of Ω_0 without suffering a degradation in noise performance due to the finite bandwidth of the squeezing. An absolute improvement in sensitivity of the absorption measurement in our experiment can be obtained by using a larger waist and therefore higher power for the probe beam (for fixed intensity) as well as by narrowing the detection bandwidth (however, these measures enhance sensitivity equally for both coherent-state and squeezed-state spectroscopy).

There are as well a variety of more fundamental issues related to the use of squeezed light in FM spectroscopy that need to be addressed in more detail. One is a limitation associated with the size of the modulation index, for which the data in Fig. 9 are relevant. Another is the existence of limits of the type discussed in [33] associated with the dephasing of squeezing due to the dispersion of the atomic vapor. However, in distinction to previous analyses of sensitivity enhancements with squeezed light, the nonlinear response of the medium must itself be considered for very large degrees of squeezing. Apart from extensions of the quantum limits to precision measurement, our source should also find gainful employment in the exploration of a number of exciting problems in optical physics related to the nature of fundamental radiative processes in the presence of squeezed light.

Acknowledgements. We gratefully acknowledge the contributions of J.L. Hall to this research program. This work was supported by the National Science Foundation (PHY-98014547), by the Office of Naval Research (N00014-90-J-1058), and by the Venture Research Unit of British Petroleum.

References

1. G.T. Milburn: Optica Acta **31**, 671 (1984)
2. C.W. Gardiner: Phys. Rev. Lett. **56**, 1917 (1986)
3. H.J. Carmichael: A.S. Lane, D.F. Walls: Phys. Rev. Lett. **58**, 2539 (1987)
4. H. Ritsch, P. Zoller: Phys. Rev. Lett. **61**, 1097 (1988)
   S. An, M. Sargent, D.F. Walls: Opt. Commun. **67**, 373 (1988)
5. A.S. Parkins, C.W. Gardiner: Phys. Rev. A **40**, 2534 (1989)
6. G.T. Milburn: Phys. Rev. A **34**, 4882 (1986)
7. C.M. Savage: Quantum Opt. **2**, 89 (1990)
   G. S. Agarwal, S.D. Gupta: Phys. Rev. A **39**, 2961 (1989)
   A.S. Parkins: Phys. Rev. A **42**, 4532 (1990)
8. A.S. Parkins, C.W. Gardiner: Phys. Rev. A **40**, 3796 (1989)
   J.M. Courty, S. Reynaud: Europhys. Lett. **10**, 237 (1989)
   P.R. Rice, L.M. Pedrotti: J. Opt. Soc. Am. B (1992)
9. J. Gea-Banacloche: Phys. Rev. Lett. **59**, 543 (1987)
   M. A. M. Marte, H. Ritsch, D.F. Walls: Phys. Rev. A **38**, 3577 (1988)
   C. Ginzel, R. Schack, A. Schenzle: J. Opt. Soc. Am. B **8**, 1704 (1991)
10. T.A.B. Kennedy, D.F. Walls: Phys. Rev. A **42**, 3051 (1990)
    P. Galatola, L.A. Lugiato, M.G. Porreca, P. Tombesi: Opt. Commun. **81**, 175 (1991)

11. M. Xiao, L.A. Wu, H.J. Kimble: Phys. Rev. Lett. **59**, 278 (1987)
12. P. Grangier, R.E. Slusher, B. Yurke, A.La Porta: Phys. Rev. Lett. **59**, 2153 (1987)
13. M. Xiao, L.A. Wu, H.J. Kimble: Opt. Lett. **13**, 476 (1988)
14. B. Yurke, E.A. Whittaker: Opt. Lett. **12**, 236 (1987)
15. "Ultrasensitive Spectroscopy": J. Opt. Soc. Am. B **2**, 1427–1593 (1985)
16. J.L. Hall, H.G. Robinson, T. Baer, L. Holberg: In *Advances in Laser Spectroscopy*, ed. by F.T. Arecchi, F. Strumia, H. Walther (Plenum, New York 1983) p. 99
17. G.C. Bjorklund, M.D. Levenson, W. Lenth, C. Ortiz: Appl. Phys. B **32**, 145 (1983)
18. L.A. Wu, M. Xiao, H.J. Kimble. J. Opt. Soc. Am. B **4**, 1465 (1987)
19. M.J. Collett, C.W. Gardiner: Phys. Rev. A **30**, 1386 (1984)
20. M.J. Collett, D.F. Walls: Phys. Rev. A **32**, 2887 (1985)
21. H.J. Kimble: In *Fundamental Systems in Quantum Optics*, ed. by J. Dalibard, J.M. Raimond, J. Zinn-Justin (Elsevier, Amsterdam 1992)
22. H.P. Yuen, V.W.S. Chan: Opt. Lett. **8**, 177 (1983)
B.L. Schumaker: Opt. Lett. **9**, 189 (1984)
23. R.W.P. Drever, J.L. Hall, F.V. Kowalski, J. Hough, G.M. Ford, A.J. Munley, M. Ward: Appl. Phys. B **31**, 97 (1983)
24. E.S. Polzik H.J. Kimble: Opt. Lett. **16**, 1400 (1991)
25. L.A. Wu, H.J. Kimble: J. Opt. Soc. Am. B **2**, 697 (1985)
26. T. Kardos. Broomer Laboratories, Islip, NY
27. R. Lalezari: PMS Electro-Optics, Boulder, CO
28. G. Mizell: Virgo Optics, Port Richey, FL
29. R.L. Byer: In *Quantum Electronics: A Treatise*, ed. by H. Rabin, C.L. Tang (Academic, New York 1975) Vol. 1, Part B, pp. 587
30. E.S. Polzik, H.J. Kimble: Technical Digest, Compact Blue-Green Laser Meeting, February 1992, Santa Fe, NM, paper ThD6
31. A. Schenzle, R.G. Devoe, R. G. Brewer: Phys. Rev. A**25**, 2606 (1982)
32. M.D. Levenson, S.S. Kano: In *Introduction to Nonlinear Laser Spectroscopy* (Academic, Boston 1988) Chap. 3
33. C.M. Caves: Phys. Rev. D **23**, 1963 (1981)
34. M. Gehrtz, G.C. Bjorkland, E.A. Whittaker: J. Opt. Soc. Am. B **2**, 1510 (1985)
35. N.C. Wong, J.L. Hall: J. Opt. Soc. Am. B **2**, 1527 (1985)
36. The electronics for the photodetectors were designed by J.L. Hall and fabricated by T. Brown at the Joint Institute for Laboratory Astrophysics, Boulder, CO
37. J. Gea-Banacloche, G. Leuchs: J. Opt. Soc. Am. B **4**, 1667 (1987)
38. E.S. Polzik, J.C. Carri, H.J. Kimble: Phys. Rev. Lett. **68**, 3020 (1992)